IOP PUBLISHING JOURNAL OF PHYSICS: CONDENSED MATTER
J. Phys.: Condens. Matter **25** (2013) 435302 (6pp) doi:10.1088/0953-8984/25/43/435302

Theoretical investigation of the electronic structure and quantum transport in the graphene–C(111) diamond surface system

Daniele Selli[1], Igor Baburin[1], Stefano Leoni[1], Zhen Zhu[2], David Tománek[2] and Gotthard Seifert[1]

[1] Institut für Physikalische Chemie, Technische Universität Dresden, D-01062 Dresden, Germany
[2] Physics and Astronomy Department, Michigan State University, East Lansing, MI 48824, USA

E-mail: Gotthard.Seifert@chemie.tu-dresden.de

Received 31 July 2013, in final form 3 September 2013
Published 4 October 2013
Online at stacks.iop.org/JPhysCM/25/435302

Abstract
We investigate the interaction of a graphene monolayer with the C(111) diamond surface using *ab initio* density functional theory. To accommodate the lattice mismatch between graphene and diamond, the overlayer deforms into a wavy structure that binds strongly to the diamond substrate. The detached ridges of the wavy graphene overlayer behave electronically as free-standing polyacetylene chains with delocalized π electrons, separated by regions containing only sp^3 carbon atoms covalently bonded to the (111) diamond surface. We performed quantum transport calculations for different geometries of the system to study how the buckling of the graphene layer and the associated bonding to the diamond substrate affect the transport properties. The system displays high carrier mobility along the ridges and a wide transport gap in the direction normal to the ridges. These intriguing, strongly anisotropic transport properties qualify the hybrid graphene–diamond system as a viable candidate for electronic nanodevices.

(Some figures may appear in colour only in the online journal)

Since its synthesis, graphene has been widely studied to explore potential applications in nanoelectronics. Its outstanding electronic properties, such as high carrier mobilities, have stimulated extensive research effort to utilize it in electronic devices and related applications (Novoselov *et al* 2004, 2005, Zhang *et al* 2005). However, the absence of a fundamental gap in the electronic structure of semimetallic planar graphene (Castro Neto *et al* 2009) prevents its use in most electronic devices. Nonetheless, successful methods to tune the band gap of graphene have been reported in recent studies, for example by using bilayer graphene (Castro *et al* 2007, Oostinga *et al* 2008) or by a general 1D confinement (Han *et al* 2007, Selli *et al* 2012). In addition, graphene's exceptional properties generate a keen interest in the next step leading to the next generation of Si-based hybrid electronics. Several studies have explored the behavior of the graphene monolayer interacting with different substrates including SiC, (Emtsev *et al* 2008, Xia *et al* 2012) SiO_2, (Ishigami *et al* 2007, Stolyarova *et al* 2007) and more recently quasi-pure Si(111) (Ochedowski *et al* 2012) and Si(100) (Xu *et al* 2011) surfaces. However, surprisingly little work has been done to investigate the interaction between graphene monolayers and the C(111) cubic diamond surface (Ma *et al* 2012).

The geometrical topology shown in figure 1(a) has been known to be a stable diamond surface reconstruction for some years. There is both theoretical (Iarlori *et al* 1992, Petukhov *et al* 2000, Marsili and Pulci 2010, Vanderbilt and Louie 1984) and experimental (Huisman *et al* 1998, Walter *et al* 2002, Graupner *et al* 1997) evidence that the reconstruction geometry of the C(111) surface is the Pandey π-chain (Pandey 1982). Formation of these quasi-1D chains within the topmost layer is accompanied by significant structural and bonding changes in the topmost four layers. A similar reconstruction has also been observed at the (111) surfaces of Si and Ge with the same diamond lattice (Himpsel *et al* 1984, Stekolnikov *et al* 2002). Theoretical studies (Jungnickel *et al* 1996)

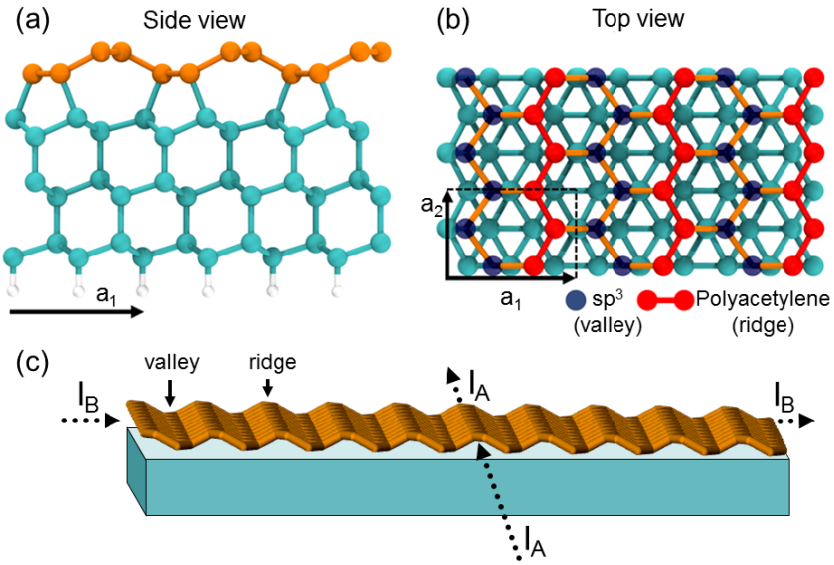

Figure 1. Optimum geometry of wavy graphene on the C(111) surface. (a) Side view and (b) top view of the equilibrium structure of the slab. The ridges of free-standing C atoms forming polyacetylene chains can be distinguished from sp^3 C atoms covalently bonded to the diamond surface. (c) Perspective view of the hybrid system, illustrating transport direction along the ridges (A) and normal to the ridges (B).

and recent observations (Ogawa *et al* 2012) indicate that this surface reconstruction may initiate a step-by-step conversion of the topmost diamond layer to graphene under ultrahigh vacuum conditions at temperatures above 1300 K. The structure of the graphene–diamond hybrid system, which we consider here, is illustrated in figure 1.

As an alternative to this 'bottom-up' perspective in the synthesis of this hybrid system, we propose a complementary 'top-down' approach by pressing a graphene monolayer onto the (111) surface of diamond. We believe that covalent graphene–diamond bonding may be induced in this way, since the interface morphology is related to the morphology of graphite that had been subject to cold compression (Selli *et al* 2011, Oganov and Glass 2006). M-carbon (Boulfelfel *et al* 2012, Wang *et al* 2012), a new carbon allotrope that was postulated previously and observed to form as the main product of the cold compression process, displays an alternating sequence of odd carbon rings (pentagons and heptagons) that covalently connect adjacent graphene layers in a characteristic '5 + 7' pattern. This new modification has the same ring topology as the first three layers of the structure shown in figure 1(a), corroborating the hypothesis of a possible synthesis via compression of graphene over a C(111) surface at a certain pressure regime.

The equilibrium morphology of the graphene–diamond interface was determined by means of *ab initio* density functional theory (DFT) calculations. In analogy with recent results (Tayran *et al* 2013) for graphene on Si(111), where the lattice mismatch was accommodated by the overlayer forming a wavy pattern, we found that the lower mismatch between graphene and the diamond C(111) surface also causes deformation of graphene to a wavy structure. This morphology, which we find to be more stable than planar graphene subject to in-layer compression, contains free-standing polyacetylene chains. Due to a sterically suppressed Peierls distortion, these chains contain delocalized π-electrons at the Fermi level. The polyacetylene chains at the ridges are separated by valley regions, which are covalently σ-bonded to the substrate, as seen in figure 1. As we will show, this bonding configuration severely affects the electronic structure of pristine, free-standing graphene. The superstructure in the hybrid system causes a pronounced anisotropy in the ballistic transport characteristic of the graphene overlayer. Optimum geometry, stability and electronic properties of the hybrid system were investigated at the DFT level of theory, as implemented in the SIESTA simulation package (Soler *et al* 2002). The (111) surface was modeled by a six-layer slab of cubic diamond with the (111) surface, saturated with hydrogen at the bottom and connected to a graphene monolayer at the top. To avoid interactions between the simulation cell replicas, the slabs were separated by a 15 Å thick vacuum region. The optimized geometry is shown in figure 1(a). We used the local density approximation to DFT with the Ceperley–Alder (Ceperley and Alder 1980) exchange–correlation functional as parameterized by Perdew and Zunger (1981) norm-conserving Troullier–Martins pseudopotentials (Troullier and Martins 1991) and a localized basis set of double-ζ orbitals including polarization functions. The charge density was represented on a real-space grid with an energy cutoff of 200 Ryd. Geometries were relaxed until a maximum force of 0.02 eV $Å^{-1}$ on the atoms was reached. The reciprocal space was sampled with a fine 60 × 1 × 60 Monkhorst–Pack $\boldsymbol{k}$-point grid (Monkhorst and Pack 1976). Quantum transport calculations for this system were performed using the nonequilibrium Green's function scheme (NEGF) as implemented in the TranSIESTA code (Brandbyge *et al* 2002). The schematic structure in figure 1(c) shows the two transport directions we considered, namely (A) along or (B) normal to the ridges of the wavy graphene. We used

a two-probe model and calculated electronic transport for the optimized structures using a single-ζ basis that included polarization functions, 200 Ryd for the energy mesh cutoff and a $120 \times 1 \times 4$ $\boldsymbol{k}$-point grid.

The optimized graphene/C(111) superlattice with the smallest 2×1 cell of the substrate is shown in figure 1. The rectangular surface unit cell, delimited by the lattice vectors $\mathbf{a}_1$ and $\mathbf{a}_2$, contains four carbon atoms in the graphene layer, 12 C atoms in the substrate slab representing cubic diamond, and two H atoms saturating the bottom of the C(111) slab. In order to identify the most stable adsorption geometry, we have investigated the relative stability of $2 \times 1, 4 \times 1$ and 6×1 supercells of the substrate lattice that provide additional structural degrees of freedom. Our results show that the '5 + 7' bonding topology associated with covalent graphene–diamond bonds occurs in all adsorption geometries, including the largest supercells. Carbon atoms in the valleys of the wavy graphene structure change their character from sp^2 to sp^3 upon forming covalent bonds to the diamond surface, with 1.59 Å long bonds comparable to 1.54 Å long covalent bonds in cubic diamond. The C–C bond length in detached graphene ridges is close to 1.43 Å. This indicates the presence of sp^2 hybridized carbon chains, where a sterically suppressed Peierls distortion keeps the electrons delocalized.

Deforming planar graphene to a wavy structure to achieve epitaxy requires an energy investment of ≈0.74 eV, which is less than when subjecting the layer to in-plane compression. Buckling brings along a significant energy gain, since it is accompanied by the formation of strong σ bonds between the overlayer and the substrate. The attachment process is exothermic, thus thermodynamically viable, if $\Delta E = E_{\mathrm{tot,graphene/diamond}} - (E_{\mathrm{tot,graphene}} + E_{\mathrm{tot,diamond}}) < 0$. In this expression, $E_{\mathrm{tot,graphene/diamond}}$ is the total energy of the relaxed wavy graphene on C(111), $E_{\mathrm{tot,graphene}}$ that of the optimized graphene monolayer, and $E_{\mathrm{tot,diamond}}$ represents the total energy of the C(111) slab. We found it useful to define the average adsorption energy per carbon atom as $E_{\mathrm{ad}} = \Delta E / N_{\mathrm{c}}$, where N_{c} is the number of carbon atoms in the graphene layer per unit cell. Our numerical result $E_{\mathrm{ad}} = -0.151$ eV indicates that the energy invested in the buckling process is more than compensated by the formation of strong σ bonds. To get a deeper insight into the energetics of this system, we compared the stability of our structure to that of previously proposed alternative geometries (Ma *et al* 2012) H, T and B that contain planar graphene in the overlayer. We find $E_{\mathrm{ad}} = -0.0208$ eV for the 'staggered configuration' H, $E_{\mathrm{ad}} = -0.0196$ eV for the 'eclipsed configuration' T, and $E_{\mathrm{ad}} = -0.0185$ eV for the 'shifted configuration' B, in qualitative agreement with (Ma *et al* 2012). The significantly stronger bonding found for wavy graphene on diamond confirms that our proposed graphene–C(111) hybrid structure should better represent the observable equilibrium geometry.

Next, we have carefully analyzed the electronic structure and determined ballistic electron transport in the optimized structure with the smallest 2×1 unit cell. We found the corrugation of about 0.73 Å of the wavy graphene normal to the surface to be enough to electronically decouple the ridge atoms in wavy graphene from carbon atoms at the surface of diamond. The electronic density of states (DOS) and projected density of states (PDOS) at ridge and valley sites of graphene in our system are shown in figure 2. In comparison to the DOS of planar graphene, shown by the dotted blue line in figure 2(a), which reflects the Dirac cone structure at E_{F}, the DOS of wavy graphene, shown by the dashed red line in figure 2(a), is higher near E_{F} due to the reduced ppπ interactions in the direction normal to the ridges. Furthermore, peaks in the DOS at ±2 eV from the Fermi level, reminiscent of van Hove singularities, are an indication of quasi-1D confinement. More detailed insight can be gained by analyzing the projected density of states for carbon atoms at the ridges and in the valleys of the wavy graphene layer, defined in figure 2(c). Careful inspection of the projected density of states reveals that the two inequivalent sites contribute in a similar way to the total DOS. Unlike planar graphene, where the region around E_{F} has exclusive p_z character, we find a significant contribution of p_x orbitals to the electronic state near E_{F} in wavy graphene. When wavy graphene attaches to diamond, C atoms in the valley bond covalently to the substrate and do not contribute electronically to states near the Fermi level. The charge accumulation in bonds connecting the 'valley' graphene C atom to three in-layer atoms and one C atom in the substrate are characteristic of sp^3 bonding found in the insulating diamond structure. As seen in figure 2(b), the character of states near E_{F} becomes dominated by p_z orbitals of C atoms at the ridge. These contributions add up to the total DOS of the hybrid system, shown by the black solid lines in figures 2(a) and (b). Unlike semimetallic graphene or insulating diamond, the hybrid graphene–diamond system is metallic. The van Hove-like singularities in the DOS near the Fermi energy indicate the presence of 1D structures, which we identify as chains of carbon atoms along the ridge with a delocalized π-electron system.

Results of our quantum transport calculations are summarized in figure 3. We considered two transport geometries, namely geometry A in figures 3(a)–(c) describing transport along the ridges and geometry B in figures 3(d)–(f) describing transport normal to the ridges. We used semi-infinite leads consisting of two cell replicas of free-stranding wavy graphene in geometry A and of one cell replica in geometry B. The scattering region was constructed of three unit cells of wavy graphene on C(111). One additional wavy graphene cell has been added on each side in order to reduce unwanted backscattering effects at the lead–scattering junction. The dangling bonds of the diamond slab have been saturated with H atoms. In our calculation, both leads and the scattering region are periodic normal to the transport direction.

The calculated transmission spectra G(E) of the graphene–diamond system are compared to transport results for free-standing wavy and planar graphene in figure 3(c) for geometry A and in figure 3(f) for geometry B. Our results for geometry A indicate a small increase in transmittance along the ridges of free-standing wavy graphene in comparison to free-standing planar graphene in a ≈0.5 eV wide energy window around E_{F}. We observe transmittance

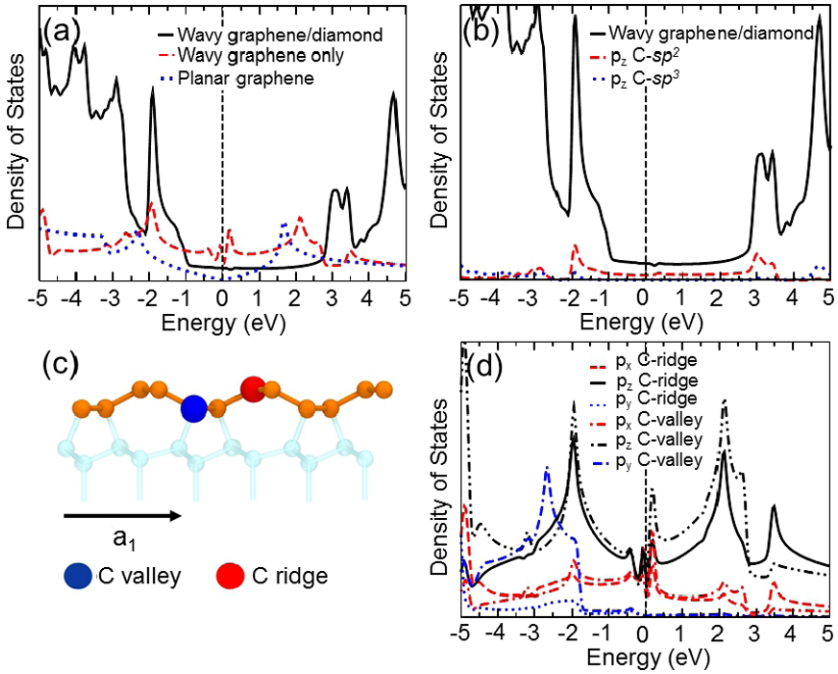

Figure 2. Electronic structure of graphene/C(111). (a) Electronic density of states (DOS) of graphene/C(111) (solid black line), free-standing wavy graphene (dashed red line) and free-standing planar graphene (dotted blue line). (b) DOS of graphene/C(111) (solid black line) and the projected electronic density of state (PDOS) onto p_z orbitals of graphene C atoms at the ridge (dashed red line) and in the valley (dotted blue line). (c) Characterization of the ridge and valley sites in the side view of the graphene/C(111) structure. (d) PDOS associated with p_x (red lines), p_y (blue lines) and p_z (black lines) states of graphene C atoms in valley and ridge sites. $E = 0$ denotes the position of the Fermi level in (a), (b) and (d).

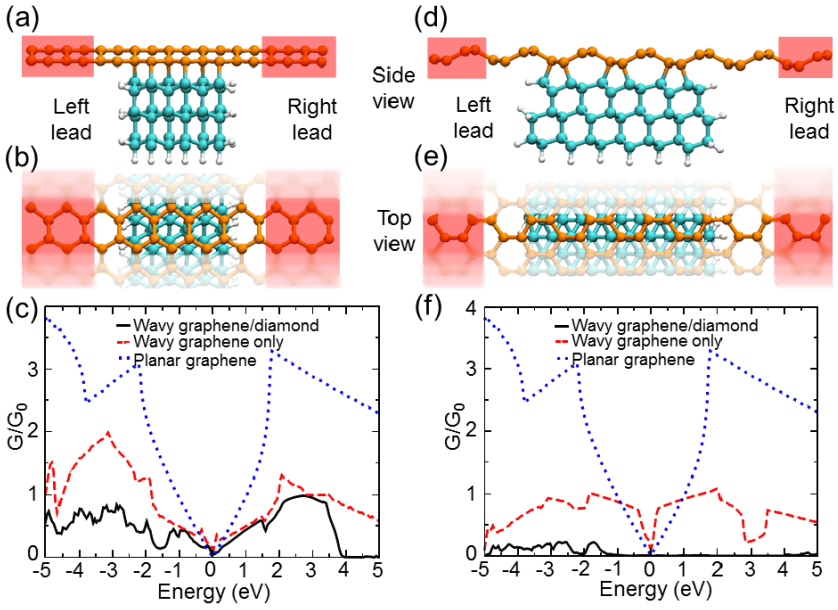

Figure 3. Geometry and numerical results of quantum transport calculations. Transport along the ridges in geometry A ((a)–(c)) is compared to transport normal to the ridges in geometry B ((d)–(f)). (a), (d) Top and (b), (e) side views of the structure used in the calculations. A central graphene–C(111) scattering region is connected to two semi-infinite leads consisting of free-standing wavy graphene. (c), (f) Transmission spectra with drain–source bias $V_{ds} = 0$ for the two geometries, with $E = 0$ representing carriers injected at the Fermi level. (The conductance is given in units of G_0 per unit cell in the direction normal to the transport direction.)

reduction outside this energy window. Further suppression of transmittance occurs when wavy graphene is bonded to the diamond substrate, indicating that the C(111) surface acts as a weak scatterer. Nonetheless, the system remains metallic, as already suggested by our DOS results presented in figure 2(a). As anticipated, the 1D transport channel is formed by the π electron system of the carbon chains along the ridges.

The situation is dramatically different in geometry B, where the transport direction is normal to the ridges. Also in this geometry, our results in figure 2(f) indicate

enhanced transmittance of free-standing wavy graphene near E_F in comparison to free-standing planar graphene. This enhancement can be attributed to the contribution of ppσ states, notably the p_x orbitals, to the DOS of wavy graphene at the Fermi energy. Attaching the wavy graphene overlayer to the C(111) surface changes the transport behavior drastically, as it opens a ≈5.5 eV wide transport gap, which is very close to the fundamental band gap of diamond. This strong change indicates that the diamond substrate, when covalently bonded to the wavy graphene overlayer, acts as a strong scattering center that efficiently suppresses transport near E_F in geometry B. Hence, the hybrid system displays a striking anisotropy in its transport behavior.

Thus, the surface can be subdivided into 'conducting nanowire regions' separated by insulating regions. In the direction along the ridges the graphene–diamond system behaves as a metal due to the conducting π-system eigenchannels, whereas in the direction normal to the ridges the system behaves as a wide-gap insulator, since the conducting channels contain only sp^3 carbon atoms in the direction of transport.

It is intriguing to compare the electronic and transport properties of graphene on C(111) to those of graphene bonded to the Si(111) substrate (Tayran *et al* 2013) with the same diamond lattice structure. The two systems differ in two major respects. For one, the lattice constant of carbon diamond is significantly smaller than that of silicon, which results in a different interface morphology and a larger fraction of graphene atoms covalently bonding to the substrate. Even though graphene forms a wavy structure both on diamond and on silicon to maintain epitaxy, the structure of the free-standing ridges is different. In graphene on Si(111), the ridges contain paraphenylene chains, whereas graphene ridges on C(111) contain polyacetylene chains with a system of delocalized π electrons. The different ridge and valley morphologies of graphene on Si(111) and C(111) are responsible for differences in the transport along the ridge direction. Unlike the case on C(111), the valleys of graphene on Si(111) contain not only sp^3 carbon atoms but also short butadiene segments (Tayran *et al* 2013). Since both Si and C(diamond) as substrate material have a fundamental band gap, transport through the scattering region normal to the ridges is limited by the interface region containing valley C atoms bonded to the substrate, resulting in a significant conductance reduction. In the graphene–diamond hybrid system, these regions contain only sp^3 carbon atoms, which completely block transmission within a wide transport gap that coincides with the fundamental gap of the substrate. The different morphology of the graphene valleys on Si(111) allows a partial transmission of electrons at energies within the fundamental band gap of the substrate.

In conclusion, we have studied the equilibrium morphology, stability and electronic structure of the interface between a graphene monolayer and the diamond C(111) surface using *ab initio* density functional calculations. We found that the optimum epitaxial interface morphology contains a wavy graphene structure that is covalently bonded to the substrate.

Whereas previous work (Ma *et al* 2012) considers an artificially compressed planar graphene overlayer on C(111), which is an unstable geometry, our finding is that flexural distortion to a wavy graphene overlayer offers a more stable epitaxial geometry. The optimum wavy structure, shown in figure 1, provides a favorable structural anisotropy. The detached ridges of the wavy graphene overlayer behave electronically as free-standing polyacetylene chains with delocalized π electrons, separated by regions with sp^3 carbon atoms covalently bonded to the (111) diamond surface. We have also performed a quantum transport calculation in order to elucidate how the deformation of the graphene layer and its bonding to the diamond substrate changes its conductance in comparison to a free-standing planar graphene monolayer. Our results show a strong anisotropy in the transmittance, with high carrier mobility along the ridges and a wide transport gap in the direction normal to the ridges. The high mobility regions at the ridges are polyacetylene chains containing delocalized π electrons. These regions are separated by graphene valleys containing sp^3 carbon atoms that are covalently bonded to the diamond substrate. The 'top-down' perspective to the Pandey chain diamond surface reconstruction permits a real nanoengineering feasibility for such an electronic device, which is currently the focus of experimental investigations (Yu *et al* 2012). The intriguing, strongly anisotropic transport properties qualify the hybrid graphene–C(111) system as a viable candidate for a new generation of high-performance electronic nanodevices for applications including topological logic switches in future nanoscale circuitry.

Acknowledgments

DS and SL thank the DFG for the support under the priority project SPP 1415, as well as ZIH Dresden for the allocation of computational resources. ZZ and DT were supported by National Science Foundation Cooperative Agreement No. EEC-0832785, titled 'NSEC: center for high-rate nanomanufacturing'. We thank M Baldoni and C Tayran for inspiring discussions related to the graphene–Si(111) system.

References

Boulfelfel S E, Oganov A R and Leoni S 2012 Understanding the nature of 'superhard graphite' *Sci. Rep.* **2** 471

Brandbyge M, Mozos J L, Ordejon P, Taylor J and Stokbro K 2002 Density-functional method for nonequilibrium electron transport *Phys. Rev.* B **65** 165401

Castro E V, Novoselov K S, Morozov S V, Peres N M R, Dos Santos J M B L, Nilsson J, Guinea F, Geim A K and Neto A H C 2007 Biased bilayer graphene: semiconductor with a gap tunable by the electric field effect *Phys. Rev. Lett.* **99** 216802

Castro Neto A H, Guinea F, Peres N M R, Novoselov K S and Geim A K 2009 The electronic properties of graphene *Rev. Mod. Phys.* **81** 109–62

Ceperley D M and Alder B J 1980 Ground-state of the electron-gas by a stochastic method *Phys. Rev. Lett.* **45** 566–9

Emtsev K V, Speck F, Seyller T, Ley L and Riley J D 2008 Interaction, growth, and ordering of epitaxial graphene on SiC{0001} surfaces: a comparative photoelectron spectroscopy study *Phys. Rev.* B **77** 155303

Graupner R, Hollering M, Ziegler A, Ristein J, Ley L and Stampfl A 1997 Dispersions of surface states on diamond (100) and (111) *Phys. Rev.* B **55** 10841–7

Han M Y, Ozyilmaz B, Zhang Y B and Kim P 2007 Energy band-gap engineering of graphene nanoribbons *Phys. Rev. Lett.* **98** 206805

Himpsel F J, Marcus P M, Tromp R, Batra I P, Cook M R, Jona F and Liu H 1984 Structure-analysis of Si(111)2× 1 with low-energy electron-diffraction *Phys. Rev.* B **30** 2257–9

Huisman W J, Lohmeier M, van der Vegt H A, Peters J F, de Vries S A, Vlieg E, Etgens V H, Derry T E and van der Veen J F 1998 Evidence for tilted chains on the diamond (111)-(2× 1) surface *Surf. Sci.* **396** 241–52

Iarlori S, Galli G, Gygi F, Parrinello M and Tosatti E 1992 Reconstruction of the diamond (111) surface *Phys. Rev. Lett.* **69** 2947–50

Ishigami M, Chen J H, Cullen W G, Fuhrer M S and Williams E D 2007 Atomic structure of graphene on SiO_2 *Nano Lett.* **7** 1643–8

Jungnickel G, Porezag D, Frauenheim T, Heggie M I, Lambrecht W R L, Segall B and Angus J C 1996 Graphitization effects on diamond surfaces and the diamond/graphite interface *Phys. Status Solidi* a **154** 109–25

Ma Y D, Dai Y, Guo M and Huang B B 2012 Graphene–diamond interface: gap opening and electronic spin injection *Phys. Rev.* B **85** 235448

Marsili M and Pulci O 2010 The fascinating physics of carbon surfaces: first-principles study of hydrogen on C(001), C(111) and graphene *J. Phys. D: Appl. Phys.* **43** 374016

Monkhorst H J and Pack J D 1976 Special points for Brillouin-zone integrations *Phys. Rev.* B **13** 5188–92

Novoselov K S, Geim A K, Morozov S V, Jiang D, Katsnelson M I, Grigorieva I V, Dubonos S V and Firsov A A 2005 Two-dimensional gas of massless Dirac fermions in graphene *Nature* **438** 197–200

Novoselov K S, Geim A K, Morozov S V, Jiang D, Zhang Y, Dubonos S V, Grigorieva I V and Firsov A A 2004 Electric field effect in atomically thin carbon films *Science* **306** 666–9

Ochedowski O, Begall G, Scheuschner N, El Kharrazi M, Maultzsch J and Schleberger M 2012 Graphene on Si(111)7× 7 *Nanotechnology* **23** 405708

Oganov A R and Glass C W 2006 Crystal structure prediction using *ab initio* evolutionary techniques: principles and applications *J. Chem. Phys.* **124** 244704

Ogawa S, Yamada T, Ishizduka S, Yoshigoe A, Hasegawa M, Teraoka Y and Takakuwa Y 2012 Vacuum annealing formation of graphene on diamond C(111) surfaces studied by real-time photoelectron spectroscopy *Japan. J. Appl. Phys.* **51** 11PF02

Oostinga J B, Heersche H B, Liu X L, Morpurgo A F and Vandersypen L M K 2008 Gate-induced insulating state in bilayer graphene devices *Nature Mater.* **7** 151–7

Pandey K C 1982 New dimerized-chain model for the reconstruction of the diamond (111)-(2× 1) surface *Phys. Rev.* B **25** 4338–41

Perdew J P and Zunger A 1981 Self-interaction correction to density-functional approximations for many-electron systems *Phys. Rev.* B **23** 5048–79

Petukhov A V, Passerone D, Ercolessi F, Tosatti E and Fasolino A 2000 (Meta) stable reconstructions of the diamond (111) surface: interplay between diamond and graphite like bonding *Phys. Rev.* B **61** 10590–3

Selli D, Baburin I A, Martonak R and Leoni S 2011 Superhard sp(3) carbon allotropes with odd and even ring topologies *Phys. Rev.* B **84** 161411

Selli D, Baldoni M, Sgamellotti A and Mercuri F 2012 Redox-switchable devices based on functionalized graphene nanoribbons *Nanoscale* **4** 1350–4

Soler J M, Artacho E, Gale J D, Garcia A, Junquera J, Ordejon P and Sanchez-Portal D 2002 The SIESTA method for *ab initio* order-N materials simulation *J. Phys.: Condens. Matter* **14** 2745–79

Stekolnikov A A, Furthmuller J and Bechstedt F 2002 Absolute surface energies of group-IV semiconductors: dependence on orientation and reconstruction *Phys. Rev.* B **65** 115318

Stolyarova E, Rim K T, Ryu S M, Maultzsch J, Kim P, Brus L E, Heinz T F, Hybertsen M S and Flynn G W 2007 High-resolution scanning tunneling microscopy imaging of mesoscopic graphene sheets on an insulating surface *Proc. Natl Acad. Sci. USA* **104** 9209–12

Tayran C, Zhu Z, Baldoni M, Selli D, Seifert G and Tomanek D 2013 Optimizing electronic structure and quantum transport at the graphene–Si(111) interface: an *ab initio* density-functional study *Phys. Rev. Lett.* **110** 176805

Troullier N and Martins J L 1991 Efficient pseudopotentials for plane-wave calculations. 2. Operators for fast iterative diagonalization *Phys. Rev.* B **43** 8861–9

Vanderbilt D and Louie S G 1984 Total energy minimization for diamond (111) surfaces—support for an undimerized Pi-bonded chain reconstruction *Phys. Rev.* B **29** 7099–101

Walter S, Bernhardt J, Starke U, Heinz K, Maier F, Ristein J and Ley L 2002 Geometry of the (2× 1) reconstruction of diamond (111) *J. Phys.: Condens. Matter* **14** 3085–92

Wang Y J, Panzik J E, Kiefer B and Lee K K M 2012 Crystal structure of graphite under room-temperature compression and decompression *Sci. Rep.* **2** 520

Xia C, Watcharinyanon S, Zakharov A A, Yakimova R, Hultman L, Johansson L I and Virojanadara C 2012 Si intercalation/ deintercalation of graphene on 6H-SiC(0001) *Phys. Rev.* B **85** 045418

Xu Y, He K T, Schmucker S W, Guo Z, Koepke J C, Wood J D, Lyding J W and Aluru N R 2011 Inducing electronic changes in graphene through silicon (100) substrate modification *Nano Lett.* **11** 2735–42

Yu J, Liu G X, Sumant A V, Goyal V and Balandin A A 2012 Graphene-on-diamond devices with increased current-carrying capacity: carbon sp(2)-on-sp(3) technology *Nano Lett.* **12** 1603–8

Zhang Y B, Tan Y W, Stormer H L and Kim P 2005 Experimental observation of the quantum Hall effect and Berry's phase in graphene *Nature* **438** 201–4